2023 IEEE International Conference on Robotics and Automation (ICRA 2023)
May 29 - June 2, 2023. London, UK

Optimized Design and Analysis of Active Propeller-driven Capsule Endoscopic Robot for Gastric Examination

Yi Zhang, Weihao Wang, Wende Ke and Chengzhi Hu, *Member IEEE*

***Abstract*— Capsule endoscopic robot holds great promise for the early diagnosis of gastrointestinal diseases without causing discomfort to patients. However, currently available active capsule endoscopic robots suffer from issues such as complex structure, poor mobility, large size, and high cost, which have hindered their widespread adoption and resulted in a lower screening rate for gastrointestinal diseases. To address these challenges, this paper proposes a highly integrated propeller-driven capsule endoscopic robot (PCER) system that integrates STM32 processor, magnetic sensor, IMU, RF communication unit, and motor drive. The micro propeller of the PCER has been analyzed through finite element simulation to ensure its efficiency. FLUENT software has been utilized to simulate the fluid force acting on the PCER as it moves through a liquid medium. The results of the simulation are then used to determine the optimal pitch angle for the robot's movement. The thrust generated by the capsule robot propellers has been measured using a lever mechanism to investigate the relationship between the thrust and voltage applied to the motors. The experiments confirmed that the PCER is capable of performing flexible motions within fluid environments, such as changing pitch angle during movement, passing circular obstacles, horizontal motion, and spiral ascent. These findings demonstrate the feasibility of the proposed PCER as an effective tool for non-invasive early screening of gastrointestinal diseases.**

I. INTRODUCTION

Gastrointestinal cancers pose a significant public health challenge, being the fifth most common cancer worldwide, accounting for over one million cases and 780,000 deaths annually. This high incidence leads to a substantial burden on healthcare resources [1]–[3]. Early diagnosis of GI tumors is crucial to improving the survival time of patients [4]. The 5-year survival rate for patients with IA and IB after surgery are 94% and 88%, respectively, while the survival rate for stage IIIC patients drops to a mere 18% [3]. Identifying typical lesions of digestive tract cancer at an early stage can prevent the development of GI cancers. However, the similarity of early GI cancers symptoms to common GI diseases can pose complex challenges for patients to identify potentially cancerous growths. Conventional gastroscopy, although effective, can cause discomfort and lower patient acceptance during the examination [5]. Although anesthesia can alleviate patient discomfort during sedation, it comes with risks and requires specialized personnel to monitor patients continually throughout the procedure, making the process more time-consuming and resource-intensive. Thus, there is a critical need to develop more efficient and less invasive methods for early screening of gastrointestinal diseases, which are more patient-friendly and consume fewer healthcare resources.

The wireless capsule endoscopic robot was initially developed and manufactured by an Israeli company as an innovative swallowable endoscope device that minimizes patient discomfort during examinations [6]–[8]. Previous passive capsule endoscopic robots were limited to following the natural peristaltic movements of the gastrointestinal tract and lacked active control, resulting in a high rate of missed examinations [9]–[11].

Therefore, active control of capsule endoscopic robots is essential for precise and comprehensive inspection, and has emerged as a prominent research focus in this field [12]–[15]. Spiral-type active capsule robots use a spiral pattern on their surface to generate forward thrust. Chi et al. have developed a spiral-type capsule robot equipped with an internal permanent magnet that rotates around its own axis, enabling it to move forward under the control of an external magnetic field [16]. Liang et al. have developed a capsule endoscopic robot that utilizes a micro motor to drive the tail screw structure [17]. Zhang et al. proposed a vibrating capsule robot with multiple electromagnetic coils mounted inside that drive the capsule robot forward by controlling the current of the coils to vibrate the internal permanent magnets [18]. Zhang et al. developed a spherical capsule endoscopic robot that can be controlled by an external electromagnetic field to enable rolling in the digestive tract [19]. A magnetorheological soft capsule robot, controlled by an external magnetic field, was developed by Hua et al [20]. Gao et al. have developed an inchworm-like capsule robot [21]. This robot is equipped with legs that can expand and contract, with one of the legs being capable of moving backwards and forwards. Mahoney et al. proposed a solution that uses a robot arm to control a permanent magnet to drive the capsule robot directly [22]. Song et al. used multiple electromagnetic coils to accomplish stable levitation, attitude modulation and motion control of the capsule robot [23]. Because most actively-driven capsule endoscopic robots require contact with the lining of the

*This work is supported by the Shenzhen Science and Technology Program (Grant No. JCYJ20190809144013494), the Science and Technology Program of Guangdong (Grant No. 2021A1515011813), the Stable Support Plan Program of Shenzhen Natural Science Fund under Grant 20220815104331001, and the Special Funds for the Cultivation of Guangdong College Students' Scientific and Technological Innovation ("Climbing Program" Special Funds) (Grant No. pdjh2022b0458). This work is supported in part by the Science, Technology and Innovation Commission of Shenzhen Municipality under grant no. ZDSYS20200811143601004, and in part by the Southern Marine Science and Engineering Guangdong Laboratory (Guangzhou).

All authors are with the Shenzhen Key Laboratory of Biomimetic Robotics and Intelligent Systems, Department of Mechanical and Energy Engineering, Southern University of Science and Technology, Shenzhen, 518055, China. (corresponding email: hucz@sustech.edu.cn).

All authors are also with Guangdong Provincial Key Laboratory of Human-Augmentation and Rehabilitation Robotics in Universities, Southern University of Science and Technology, Shenzhen, 518055, China.

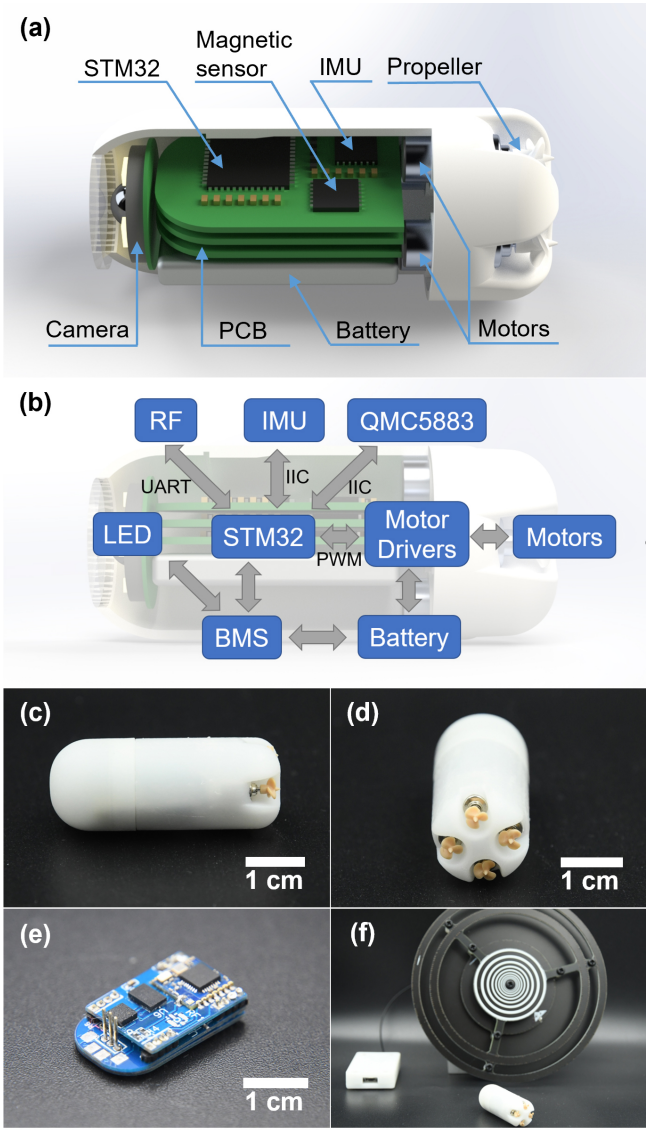

Fig. 1. (a) Schematic diagram of the internal structure of the PCER. (b) Schematic diagram of the PCER's electronic system. (c)(d) PCER prototype. (e) Printed circuit board of the PCER. (f) Signal receiver and antenna.

digestive tract to obtain forward force, these designs may not be suitable for examinations in larger spaces of the stomach. The capsule robots that use magnetic field to realize levitation require highly accurate positioning methods to achieve stable closed-loop control, which can be difficult and expensive to achieve.

To address the challenges of existing capsule endoscopic robots, we propose a new design based on miniature propellers, which offers improved efficiency and reduced cost. Section II presents the hardware structure and circuit system of the proposed PCER robot. In section III, we use computational fluid dynamics to simulate the hydrodynamic characteristics of the propeller and shell of PCER. PCER thrust measurement and motion experiments are presented in section IV to validate the overall design. Section V provides a summary of this work.

II. HARDWARE DESIGN OF THE PCER

Figure 1 illustrates the capsule endoscopic robot driven by four propellers. The current shell of the PCER is fabricated through 3D printing, utilizing resin as the primary material. Four hollow cup motors (diameter: 4 mm and length: 8 mm) are mounted at the rear of the PCER. On each motor shaft, a miniature propeller is attached. The STM32F411 micro processing unit serves as the core of the PCER's circuit, which generates PWM signals to control the motor drive IC (BDR6122T) and regulate the speed of each motor. Data from the IMU (BMI088) and magnetic sensor (QMC5883P) is transmitted via the IIC bus with the STM32F411. The radio frequency communication unit (CC2640) enables data exchange with the STM32F411 through the UART serial port. The signal receiver uses a 2.4 GHz RF signal to establish communication between the host computer and the PCER.

Propeller design is optimized and modified based on existing design maps, such as the B-σ maps and the K-J maps [24]. The map method is utilized to determine the design parameters that correspond to the outer contour and blade section characteristics, either through the pitch ratio or the advance speed coefficient. In this paper, we utilize OpenProp, an open source tool based on MATLAB, to assist in the design of propellers. OpenProp takes the chord length and thickness of the propeller blade section at different radii as input, and generates multiple three-dimensional value point data that can be fitted to a smooth propeller blade section. The centerline and thickness characteristics of the propeller blade section surface profile can be defined, usually modified according to the characteristics of the existing propeller model [25]. The 3D point data exported from MATLAB can be imported into SOLIDWORKS for modeling.

III. FLUID SIMULATION AND ANALYSIS

A. Simulation and analysis of the propeller

The simulation and analysis of the propeller were conducted using FLUENT, which offers various Reynolds Average Navier-Stokes equations (RANS) turbulence models. To accurately simulate the boundary layer with large pressure gradient and the propagation of cylindrical jet flow in the fluid, the Realizable K-ϵ turbulence model was employed [26]. However, since the turbulent flow on the surface of the propeller blade is not fully developed, the K-ϵ model with wall functions was used to deal with the flow near the wall. In still water, the Reynolds number of the fluid flowing over the surface of the propeller blades can be approximated as:

$$Re = \frac{nD^2}{\nu} \tag{1}$$

where n is the rotation speed of the propeller; D is the diameter of the propeller; ν is the dynamic viscosity coefficient of the fluid.

It is estimated that the minimum operating speed of the propeller is 2000 rpm, and the Reynolds number of the fluid on the surface of the propeller blade is around 4200, indicating a low Reynolds number turbulent flow. Scalable

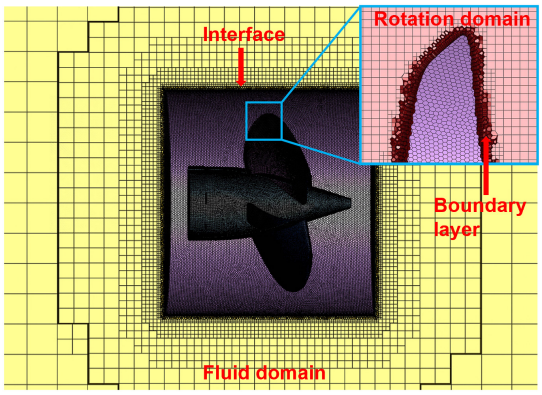

Fig. 2. The grid refinement is applied close to interface. Boundary layer mesh is unstructured grid to fit the geometrical characteristic of the propeller.

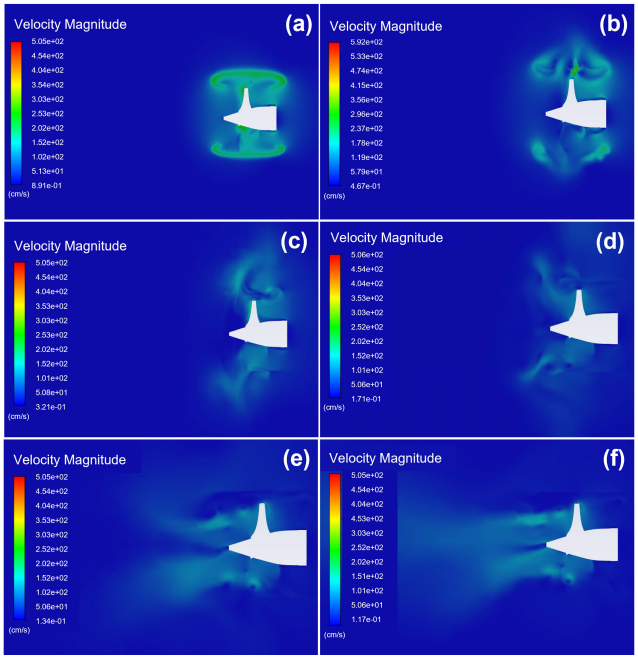

Fig. 3. Iterative cloud map showing the flow field velocity when the rotation domain has a speed of 12000 rpm, and the inlet has a speed of 0.05 m/s.

Wall Function was used to process the boundary layers grid with low Reynolds number to prevent singular values that are difficult to converge in the boundary layers [27].

To estimate the propeller thrust and torque, three mesh division methods can be used: single-moving reference frame mesh (SRF), sliding mesh, and overlapping mesh. All three methods are reliable and effective in predicting the open-water thrust characteristics of propellers [28]. SRF has the advantages of fast calculation speed and simple grid division. In this paper, SRF is used for modeling and calculation.

The model is divided into two parts, one part is the fluid domain with the propeller surface as the wall. The other part is the fluid domain that does not rotates directly, which wraps around the former part. The interface between the two domains adopts the grid share topology during mesh partitioning [29]. The fluid on the surface of the propeller and the

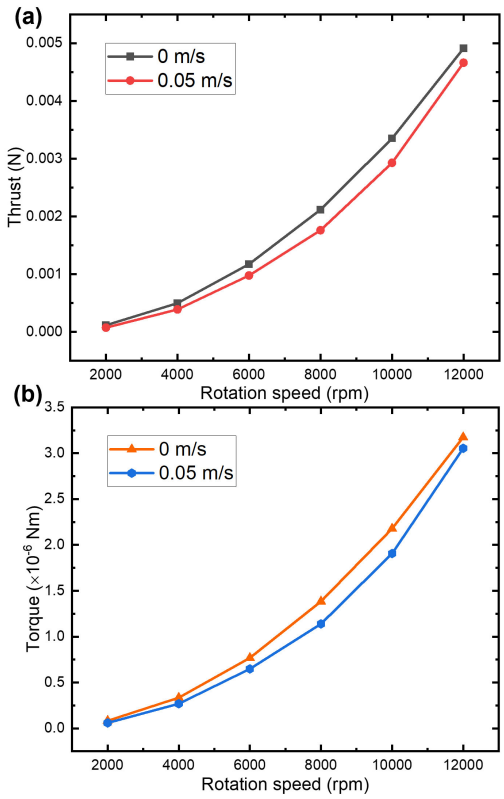

Fig. 4. (a) Relationship between propeller thrust and rotation speed at different PCER forward velocities. (b) Relationship between propeller torque and rotation speed at different PCER forward velocities.

rotation domain is relatively complex, and hence the mesh is refined [30]. The grid adopts the poly-hexcore method of fluent mesh. The structured grid and the unstructured grid are established hierarchically. This approach can divide higher-quality grids while keeping the number of grids small, improving the simulation calculation speed. As shown in Fig. 2, the number of grids is about 2,630,000. The minimum orthogonal quality of the grid is about 0.2, and the maximum skewness is about 0.6, both of which appear on the boundary layers of the propeller, meeting engineering requirements.

During capsule endoscope examination, patients need to empty their stomach and take 2 liter of water to temporarily fill the stomach. At a temperature of 20 °C, the dynamic viscosity coefficient of human gastric acid is less than 10% different from that of pure water, and the density of gastric acid is also similar to that of pure water. Therefore, the working environment of the PCER can be approximated as pure water.

The speed of rotation domain ranges from 2000 rpm to 12000 rpm. The wall of the propeller is set as a moving wall, and the rotation speed is consistent with the rotation domain. The inlet is set to velocity inlet, with respective speeds of 0 m/s and 0.05 m/s; the outlet is set to pressure outlet; the turbulent intensity of the fluid is set to 5%; the turbulent viscosity ratio is set to 10%.

The residual convergence condition is set to 10^{-5} to achieve higher simulation calculation accuracy. In simula-

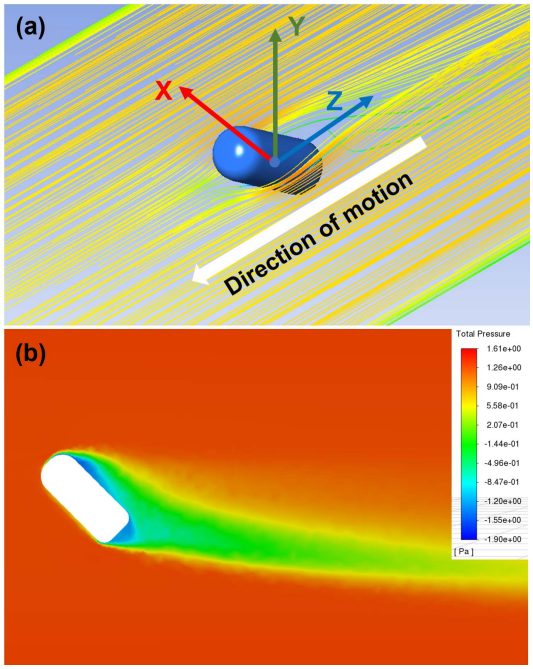

Fig. 5. (a) The motion state of the PCER and robot coordinate system. (b) Pressure distribution in the YZ-plane. PCER moves forward at 0.06 m/s with 45 degrees pitch angle. The pressure distribution shows that the fluid exerts forces on the PCER in the Z and Y directions.

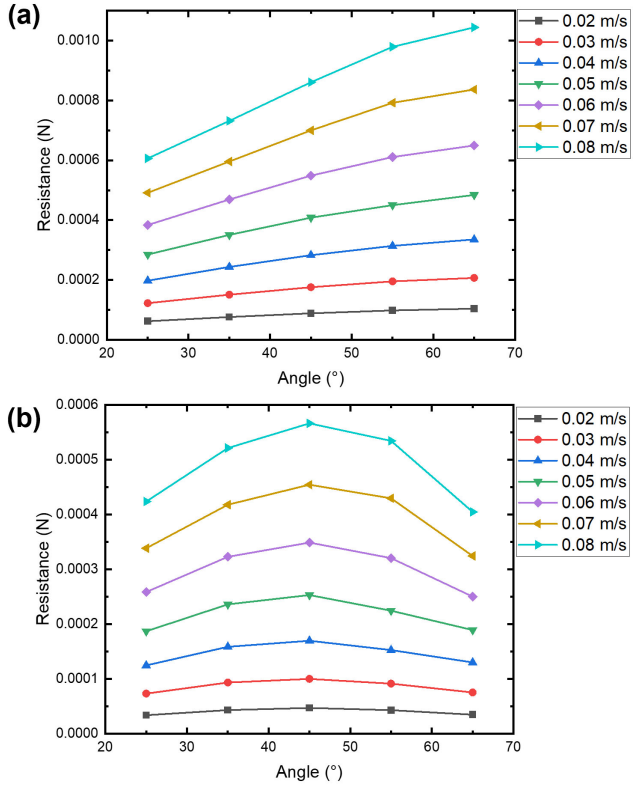

Fig. 6. (a) The component of the fluid force on the PCER in the Z-direction shows a positive correlation with the Z-directional velocity and pitch angle of the PCER's motion. (b) The component of the fluid force on the PCER in the Y-direction shows a positive correlation with the velocity in the Z-direction of the PCER. At the same speed, the component of the fluid force in the Y-direction reaches its maximum at 45 degrees pitch angle.

tion, the pressure-velocity coupling iteration scheme adopts the COUPLE method; the pressure term adopts the second-order equation; the momentum adopts the second-order upwind scheme and the turbulent kinetic energy and dissipation rate adopt the first-order upwind scheme. The initial value is set to 30 steps of iterative calculation in the hybrid initialization method. During the iterative calculation process before convergence, the velocity contour of the liquid near the propeller is shown in Fig. 3. It can be observed that the fluid initially diffuses from the rotating domain to the surroundings, and the fluid state is unstable. The propeller generates a relatively clear turbulent flow backward, and the rest of the fluid state is stable, reflecting the convergence of the results.

The results obtained by the simulation are shown in Fig. 4. When the advance speed is 0, the propeller only rotates without moving forward, the thrust and torque obtained are the largest. When the advance speed coefficient of the propeller increases, the thrust coefficient and torque coefficient decrease [31]. The propeller thrust and torque can be expresses as :

$$F = K_t \rho n^2 D^4 \tag{2}$$

$$Q = K_q \rho n^2 D^5 \tag{3}$$

where K_t and K_q are coefficients, n is the rotation speed of the propeller; D is the diameter of the propeller; ρ is the fluid density. When the advance speed remains constant and the propeller speed decreases, the advance speed coefficient increases, the coefficients K_t and K_q decreases. When the propeller has the same velocity, higher advance speed causes lower thrust and torque.

B. Simulation and analysis of PCER shell

The average density of the PCER is greater than water, and therefore it remains submerged while underwater. In addition, the position of the center of mass plays an important role in determining the pitch angle of the PCER during movement, which can significantly impact the robot's mobility performance. As shown in Fig. 5(a), the PCER is subjected to the impact of the current as it moves through the water. In the vertical plane, the impact force can be divided into a force along the Y-direction and a force in the Z-direction. The impact force in the Y-direction aids the robot in overcoming gravity. When the sum of the component of fluid force in the Y-direction, buoyancy force, and the component of the thrust generated by the propellers in the Y-direction equals the gravity of PCER, the robot is able to achieve a stable movement in the Y-direction. When the thrust generated by the PCER propellers in the Z-direction and the resistance of the fluid in the Z-direction balance each other, the robot maintains a constant speed in the Z-direction.

We use FLUENT to simulate and analyze the fluid resistance and lift force of the PCER. Figure 5(b) presents

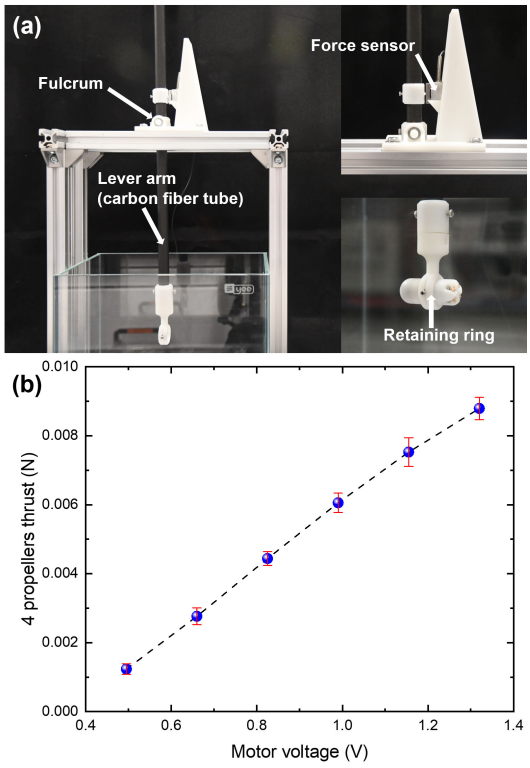

Fig. 7. (a) Device for measuring the thrust of PCER. The PCER is mounted in a fixed ring at the end and its thrust is amplified by a lever, which in turn is measured by a force sensor. (b) The thrust of the four PCER propellers shows an approximately linear relationship with the motor voltage. The same gradually increasing voltage was applied to all four motors in the experiment.

the pressure distribution of the PCER in the YZ-plane at a pitch angle of 45 degrees and a velocity of 6 cm/s. Using FLUENT's built-in force calculation tool, the force in the Y and Z directions of the PCER were quickly computed. We examined the force in the Z-direction as the pitch angle of the PCER body varied from 20 degrees to 65 degrees and the velocity changed from 2 cm/s to 8 cm/s. As illustrated in Fig. 6(a), the drag force in the Z-direction of the robot increased with the pitch angle and body speed. Therefore, the pitch angle of the PCER should not be excessively large to conserve energy consumption. On the other hand, the lift force in the Y-direction increased with speed but decreased when the pitch angle exceeded 45 degrees, as shown in Fig. 6(b). Consequently, to obtain the optimal lift effect and energy conservation while considering the forces in the Y and Z directions, the pitch angle of the PCER body should be maintained near 45 degrees.

IV. EXPERIMENTAL VALIDATION

To evaluate the thrust generated by a PCER in a liquid environment, we devised an experimental platform, as depicted in Fig. 7(a). Computational simulations have indicated that the PCER's thrust output is minimal, necessitating the application of a lever mechanism to amplify the thrust. A carbon fibre tube (diameter: 12 mm and wall thickness: 2 mm) is used as the force arm of the amplifying lever. The

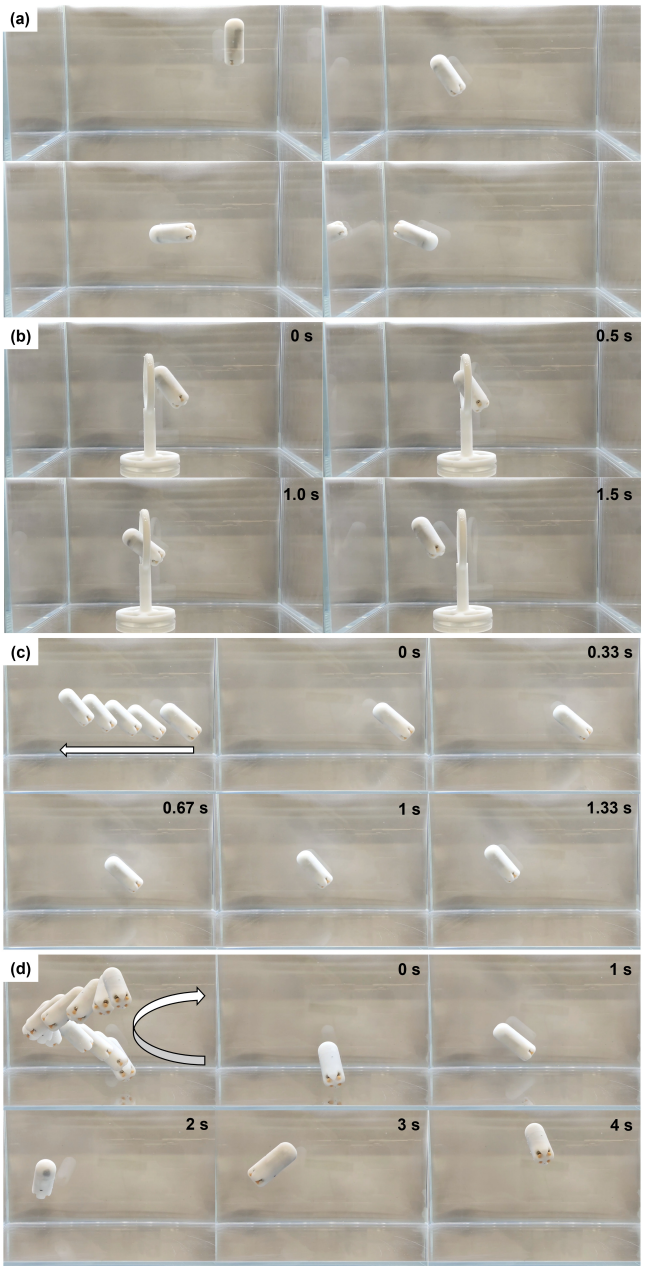

Fig. 8. (a) The pitch angle adjustments of the PCER during movement. (b) The PCER traverses a circular target with a diameter of 4 cm. (c) The PCER moves horizontally in the vertical plane. (d) The PCER completes cruise in a spiral upwards.

carbon fibre tube is fitted with a ring at the end to hold the PCER in place. The lever's power arm is 25 cm in length, while the resistance arm is 3 cm in length. After the PCER was fixed to the device, we applied the same progressively increasing voltage to the four motors and recorded the force sensor readings. The results shown in Fig. 7(b) demonstrate that the thrust of the PCER increases with increasing voltage which has good linearity.

To validate the mobility of the PCER, a simulated operating environment was created using a tank with dimensions of $220 \times 160 \times 170$ mm. The PCER's attitude and movement

direction during locomotion are controlled by the differential speed between the corresponding propellers. To prevent rotation of the capsule robot around its own axis, it is necessary to ensure that the torque on the PCER is balanced between the clockwise and counterclockwise rotating propellers. Fig. 8(a) shows the PCER changing the pitch angle of the body in a liquid environment. Through our experiments we have found that the PCER is able to achieve flexible changes in the pitch angle by manipulating the difference in thrust between the upper and lower propellers. This motion function allows doctors to observe more information during the operation of the PCER. The motion control capabilities of capsule endoscopic robots are crucial in precision examinations. To assess the control performance of the PCER, we conducted an experiment in which the capsule robot traversed a circular path. In this experiment, the PCER was initiated from the bottom of the tank, approached the target ring (4 cm in diameter), and passed through it as shown in Fig. 8(b). This experiment verifies that the PCER can precisely reach the desired position and maintain a stable control of its own motion. The horizontal and spiral movements of the capsule robot are important for achieving the robot's automatic cruise inspection function within the stomach. The horizontal motion enables multiple views of the same target height in the stomach, while the spiral upward motion realizes examination of targets at varying heights in the stomach. We validated the capability of the PCER to execute both horizontal and spiral movements in a liquid environment via experiments as shown in Fig. 8(c) and Fig. 8(d).

V. CONCLUSION

In this paper, we propose a novel capsule endoscopic robot that employs miniature propellers for locomotion. The integration of various electronic components within the limited space of the capsule robot has enabled it to perform data processing and autonomous attitude solving. The hydrodynamic performance of the miniature propeller is evaluated using finite element simulations. Additionally, the forces applied on the PCER when operating in a liquid environment are also simulated. A comprehensive analysis is conducted to determine an optimal angle of orientation for the robot's motion. In order to conduct an assessment of the performance of PCER propellers, the thrust generated by the whole machine is measured and a correlation between thrust and motor voltage is obtained. The experiment results demonstrate that the proposed capsule robot is capable of executing diverse motion functionalities, including changing attitude during movement, reaching specific targets, traversing circular obstacles, maintaining stable horizontal motion, and helical cruising motion. As a compact endoscopic robotic system, the PCER significantly reduces the dependence of existing magnetic capsule endoscopes on large equipment and lower the cost of examination, which is important for promoting early screening for gastrointestinal diseases. The innovation and utility of the PCER can be further enhanced by future research aimed at modeling the dynamics and automated control of propeller-driven capsule endoscopic robot.

ACKNOWLEDGMENT

The authors acknowledge the assistance of SUSTech Core Research Facilities and SUSTech(SIR)-Jifu Medical Robotics Joint Laboratory.

REFERENCES

[1] F. Bray, J. Ferlay, I. Soerjomataram, R. L. Siegel, L. A. Torre, and A. Jemal, "Global cancer statistics 2018: Globocan estimates of incidence and mortality worldwide for 36 cancers in 185 countries," *CA: a cancer journal for clinicians*, vol. 68, no. 6, pp. 394–424, 2018.

[2] M. Arnold, C. C. Abnet, R. E. Neale, J. Vignat, E. L. Giovannucci, K. A. McGlynn, and F. Bray, "Global burden of 5 major types of gastrointestinal cancer," *Gastroenterology*, vol. 159, no. 1, pp. 335–349, 2020.

[3] P. Rawla and A. Barsouk, "Epidemiology of gastric cancer: global trends, risk factors and prevention," *Gastroenterology Review/Przeglad Gastroenterologiczny*, vol. 14, no. 1, pp. 26–38, 2019.

[4] S. Macdonald, U. Macleod, N. C. Campbell, D. Weller, and E. Mitchell, "Systematic review of factors influencing patient and practitioner delay in diagnosis of upper gastrointestinal cancer," *British journal of cancer*, vol. 94, no. 9, pp. 1272–1280, 2006.

[5] W. Luman, "Patients' perception of transnasal gastroscopy," *Singapore medical journal*, vol. 49, no. 4, p. 339, 2008.

[6] P. Swain, "The future of wireless capsule endoscopy," *World journal of gastroenterology: WJG*, vol. 14, no. 26, p. 4142, 2008.

[7] J.-C. Saurin, N. Beneche, C. Chambon, and M. Pioche, "Challenges and future of wireless capsule endoscopy," *Clinical Endoscopy*, vol. 49, no. 1, pp. 26–29, 2016.

[8] W. El-Matary, "Wireless capsule endoscopy: indications, limitations, and future challenges," *Journal of pediatric gastroenterology and nutrition*, vol. 46, no. 1, pp. 4–12, 2008.

[9] M.-H. Meng, T. Mei, J. Pu, C. Hu, X. Wang, and Y. Chan, "Wireless robotic capsule endoscopy: State-of-the-art and challenges," in *Fifth world congress on intelligent control and automation (IEEE Cat. No. 04EX788)*, vol. 6, 2004, pp. 5561–555a.

[10] L. Liu, S. Towfighian, and A. Hila, "A review of locomotion systems for capsule endoscopy," *IEEE reviews in biomedical engineering*, vol. 8, pp. 138–151, 2015.

[11] G. Ciuti, A. Menciassi, and P. Dario, "Capsule endoscopy: from current achievements to open challenges," *IEEE reviews in biomedical engineering*, vol. 4, pp. 59–72, 2011.

[12] S. S. Mapara and V. B. Patravale, "Medical capsule robots: A renaissance for diagnostics, drug delivery and surgical treatment," *Journal of Controlled Release*, vol. 261, pp. 337–351, 2017.

[13] L. Liu, S. Towfighian, and A. Hila, "A review of locomotion systems for capsule endoscopy," *IEEE reviews in biomedical engineering*, vol. 8, pp. 138–151, 2015.

[14] Z. Huang and C. Hu, "Real-time attitude tracking of capsule endoscope based on mems imu and error analysis," in *2021 IEEE International Conference on Real-time Computing and Robotics (RCAR)*, 2021, pp. 968–973.

[15] Y. Li, Z. Huang, X. Liu, Y. Jie, C. Song, and C. Hu, "Calibrated analytical model for magnetic localization of wireless capsule endoscope based on onboard sensing," *Robotica*, p. 1–15, 2023.

[16] M. Chi, J. Zhang, R. Liu, Y. Wang, G. Nie, and X. Qian, "Coupled steering control of a low torsional torque capsule robot in the intestine," *Mechatronics*, vol. 77, p. 102596, 2021.

[17] H. Liang, Y. Guan, Z. Xiao, C. Hu, and Z. Liu, "A screw propelling capsule robot," in *2011 IEEE International Conference on Information and Automation*, 2011, pp. 786–791.

[18] J. Zhang, J. Tian, D. Zhu, Y. Liu, and S. Prasad, "Design and experimental investigation of a vibro-impact self-propelled capsule robot with orientation control," in *2022 International Conference on Robotics and Automation (ICRA)*, 2022, pp. 11 381–11 387.

[19] Y. Zhang, X. Liu, G. Liu, X. Ji, H. Yang, and Z. Liu, "Design and implementation of a highly integrated dual hemisphere capsule robot," *Biomedical Microdevices*, vol. 24, no. 1, p. 10, 2022.

[20] D. Hua, X. Liu, H. Lu, S. Sun, M. A. Sotelo, Z. Li, and W. Li, "Design, fabrication, and testing of a novel ferrofluid soft capsule robot," *IEEE/ASME Transactions on Mechatronics*, vol. 27, no. 3, pp. 1403–1413, 2021.

[21] J. Gao, Z. Zhang, and G. Yan, "Locomotion analysis of a clamper-based capsule robot in a compliant tube," *IEEE/ASME Transactions on Mechatronics*, vol. 26, no. 1, pp. 55–65, 2020.

[22] A. W. Mahoney and J. J. Abbott, "Five-degree-of-freedom manipulation of an untethered magnetic device in fluid using a single permanent magnet with application in stomach capsule endoscopy," *The International Journal of Robotics Research*, vol. 35, no. 1-3, pp. 129–147, 2016.

[23] L. Song, Y. Dai, L. Wang, W. Zhang, Y. Ji, Y. Cao, J. Wei, F. Wang, J. Zhong, J. Yang *et al.*, "Motion control of capsule robot based on adaptive magnetic levitation using electromagnetic coil," *IEEE Transactions on Automation Science and Engineering*, pp. 1–12, 2022.

[24] F. Vesting, R. Gustafsson, and R. E. Bensow, "Development and application of optimisation algorithms for propeller design," *Ship Technology Research*, vol. 63, no. 1, pp. 50–69, 2016.

[25] S. Udupa, N. Joshi, and S. Raman, "Design, analysis and control of an autonomous underwater surveillance robot," in *2017 IEEE International Conference on Consumer Electronics-Asia (ICCE-Asia)*, 2017, pp. 121–126.

[26] A. Bahatmaka, D.-J. Kim, and Y. Zhang, "Verification of cfd method for meshing analysis on the propeller performance with openfoam," in *2018 International Conference on Computing, Electronics & Communications Engineering (iCCECE)*, 2018, pp. 302–306.

[27] J. Zhou, G. Xing, and S. Zhou, "Effects of different turbulence models on simulation accuracy of the miniature super-low specific speed centrifugal pump," in *IOP Conference Series: Materials Science and Engineering*, vol. 490, no. 5, 2019, p. 052026.

[28] Q. Zhang and R. K. Jaiman, "Numerical analysis on the wake dynamics of a ducted propeller," *Ocean Engineering*, vol. 171, pp. 202–224, 2019.

[29] T. G and N. J, "Aerodynamic analysis of uav propeller with various angle of attack using computational fluid dynamics," in *2022 IEEE Silchar Subsection Conference (SILCON)*, 2022, pp. 1–7.

[30] A. Rastogi and M. Mathew, "Cavitation visualization and prediction of propeller characteristics of insean e779a propeller using sliding mesh model," in *OCEANS 2022 - Chennai*, 2022, pp. 1–8.

[31] F. Meng, C. Zhang, and Y. Zhao, "Modeling and simulation of marine propeller load," in *2016 IEEE International Conference on Mechatronics and Automation*, 2016, pp. 2371–2375.